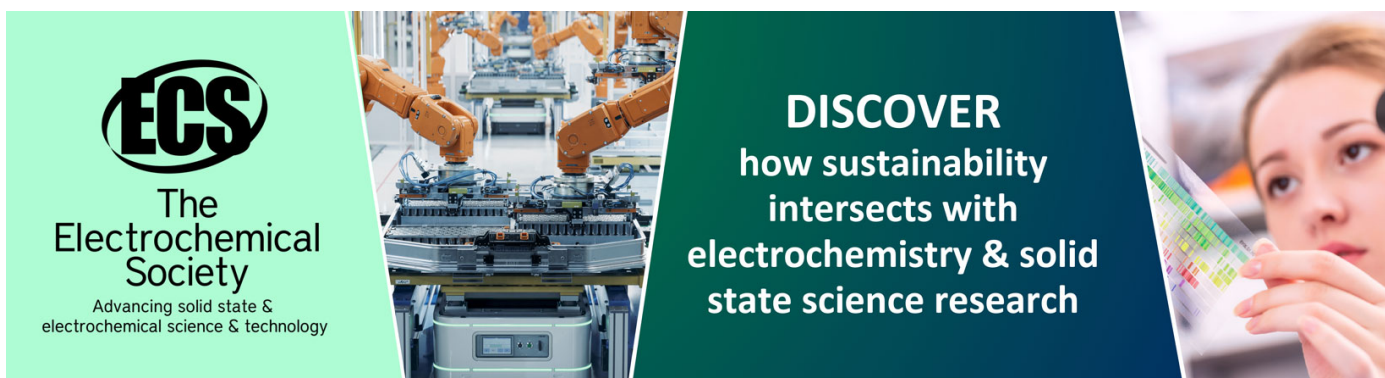# Toxicity of silver nanoparticles in zebrafish models

To cite this article: P V Asharani *et al* 2008 *Nanotechnology* **19** 255102

View the article online for updates and enhancements.

Toxicity of silver nanoparticles in zebrafish models

P V Asharani[1]**, Yi Lian Wu**[2]**, Zhiyuan Gong**[2] **and Suresh Valiyaveettil**[1,3]

[1] Department of Chemistry, Faculty of Science, National University of Singapore, 3 Science Drive 3, 117543, Singapore

[2] Department of Biological Sciences, National University of Singapore, Science Drive 4, 117543, Singapore

E-mail: chmsv@nus.edu.sg

Abstract

This study was initiated to enhance our insight on the health and environmental impact of silver nanoparticles (Ag-np). Using starch and bovine serum albumin (BSA) as capping agents, silver nanoparticles were synthesized to study their deleterious effects and distribution pattern in zebrafish embryos *(Danio rerio)*. Toxicological endpoints like mortality, hatching, pericardial edema and heart rate were recorded. A concentration-dependent increase in mortality and hatching delay was observed in Ag-np treated embryos. Additionally, nanoparticle treatments resulted in concentration-dependent toxicity, typified by phenotypes that had abnormal body axes, twisted notochord, slow blood flow, pericardial edema and cardiac arrhythmia. Ag^+ ions and stabilizing agents showed no significant defects in developing embryos. Transmission electron microscopy (TEM) of the embryos demonstrated that nanoparticles were distributed in the brain, heart, yolk and blood of embryos as evident from the electron-dispersive x-ray analysis (EDS). Furthermore, the acridine orange staining showed an increased apoptosis in Ag-np treated embryos. These results suggest that silver nanoparticles induce a dose-dependent toxicity in embryos, which hinders normal development.

1. Introduction

The toxicology of engineered nanomaterials is a relatively new and evolving field. Although the applications of nanoparticles are increasing broadly in every field, concerns about their environmental and health impacts remain unresolved. Nanoparticles have become a part of our daily life, in the form of cosmetics [1], drug delivery systems [2], therapeutics [3] and biosensors [4]. However, little is known about their biodistribution and bioactivity. Silver nanoparticles have gained much popularity on account of their antimicrobial properties [5, 6]. They are extensively used in detergents and wound dressings, which end up in the environment during waste disposal [7]. The commercial applications of the nanoparticles are accompanied by a lack of safety regulations and toxicology data. It has been reported that ultrafine particles could cause more damage than larger particles when delivered at the same concentration [8]. Most of the nanotoxicology studies were focused on *in vitro* models. Only a few research groups have dealt with aquatic *in vivo* systems [9]. Toxicology studies in *in vivo* systems carry greater significance pertaining to their diversity in physiology and anatomy. Experiments on medaka fish using fluorescent solid latex nanoparticles confirmed a homogeneous distribution of the particles [10]. Earlier reports [11–13] proved that silver nanoparticles are more lethal to cell-based *in vitro* systems than other metal nanoparticles screened. In the present study, zebrafish embryos were chosen as model systems for testing ecotoxicity of the silver nanoparticles. We have used different concentrations of Ag^+ ions, silver nanoparticles capped with BSA (Ag-BSA) and starch (Ag-starch) to monitor the developmental abnormalities induced by the nanoparticles. The capping agent (stabilizing agent) was chosen to make the nanoparticle soluble in water and to protect nanoparticles from agglomerating in the medium. The choice of starch and BSA was made in order to synthesize a water soluble and stable nanoparticle

---

[3] Author to whom any correspondence should be addressed.

suspension. Moreover, use of organic solvents and other toxic chemicals may yield highly toxic products that hinder bio-applications. The nanoparticles employed in this study were highly stable and water soluble. The extent of toxicity was measured in terms of mortality, hatching, heart rate and abnormal phenotypes. Transmission electron microscopy (TEM) of the Ag-BSA treated embryos showed a significant concentration of nanoparticles inside the nucleus.

2. Materials and methods

2.1. Synthesis of silver nanoparticles

All starting materials for the synthesis of nanoparticles were purchased from Sigma-Aldrich, unless otherwise stated. All glassware was cleaned thoroughly to ensure an endotoxin-free environment.

*2.1.1. Silver nanoparticles capped with soluble potato starch.* The starch solution was made by boiling soluble potato starch (0.28 g) in 10 ml of ultrapure water and filtering the solution through a millipore filter (0.2 μm). Starch capped silver nanoparticles were prepared by reducing silver nitrate solution (1 mM) using sodium borohydride (0.04 g) followed by the addition of the filtered starch solution, under constant stirring, at 60 °C. The color of the solution changed to dark brown with time and stirring was continued for 2 h.

2.1.2. Silver nanoparticles capped with BSA. The synthesis protocol for Ag-BSA was similar to Ag-starch, using BSA (0.1 g) as capping agent and sodium borohydride (0.025 g) as reducing agent. Nanoparticles were centrifuged and washed thoroughly in ultrapure water to remove excess capping agents. The pellet obtained after centrifugation was resuspended in 4 ml ultrapure water and lyophilized. Stock solutions (10 mg ml^{-1}) were prepared from the lyophilized pellet, sonicated and diluted using embryo water (prepared by dissolving 60 mg sea salt in one liter of water) to get the required concentrations. Stable nanoparticle suspensions were obtained in both cases.

2.2. Characterization of nanoparticles

2.2.1. TEM analysis of the nanoparticles. Stock solutions of the nanoparticles were used for TEM analysis. TEM images showed that both Ag-starch (figure 1(A)) and Ag-BSA (figure 1(B)) nanoparticles have an average size of 5–20 nm.

2.2.2. UV–vis spectrum of silver nanoparticles. Silver nanoparticles exhibit an intense brown color due to the surface plasmon resonance (SPR), which results from collective oscillations of their conduction band electrons in response to electromagnetic waves. This is well studied and reported earlier by other groups [14]. Under the UV region, Ag-nps give a characteristic absorbance band due to the excitation mode of their surface plasmons which is dependent on the nanoparticle size. These SPR bands undergo redshift or blueshift depending on the quantum size effects [14].
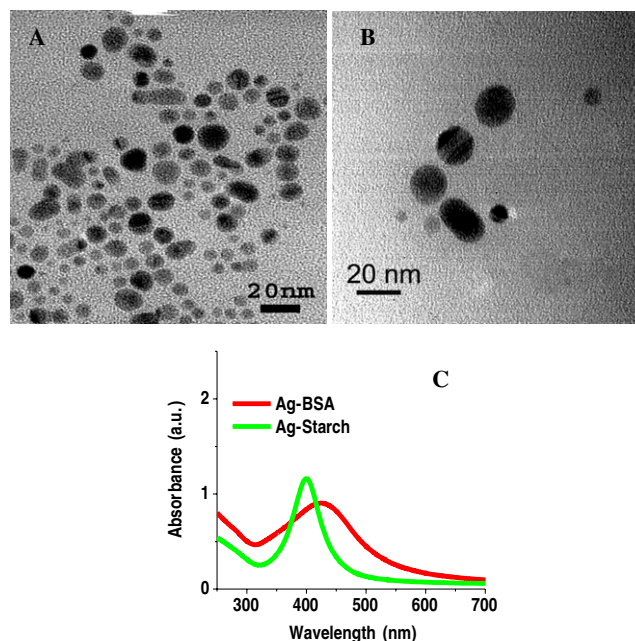
Figure 1. Characterization of nanoparticles: TEM image of Ag-starch (A) and Ag-BSA nanoparticles. The nanoparticles showed a size of 5–20 nm. UV–vis spectrum (B) of Ag-starch nanoparticles showed maximum absorbance at 400 nm whereas Ag-BSA showed a much broader peak with maximum absorbance at 424 nm.

(This figure is in colour only in the electronic version)

Hence, absorbance peaks can be used as tools to predict particle size and stability. Smaller silver nanoparticles will have an absorbance maximum around 400 nm which increases with size and disappears when particle size falls outside nanodimensions. To study the optical properties of our silver nanoparticles, the absorbance maximum of silver nanoparticles in water was measured. Ag-starch nanoparticles showed maximum absorbance at 400 nm, whereas Ag-BSA nanoparticle showed maximum absorbance at 424 nm. A narrow absorption peak around 400 nm showed that Ag-starch nanoparticles have a narrow size distribution with smaller sized particles predominating, whereas Ag-BSA nanoparticles showed a broader size distribution (predominantly bigger nanoparticles).

2.3. Collection and exposure of the embryos to nanoparticles

Zebrafish embryos were collected from the zebrafish aquarium in the Department of Biological Sciences, National University of Singapore and staged according to standard procedures [15]. For toxicity studies, 10 healthy embryos were transferred to the wells of a 24-well plate along with 1 ml of embryo water (60 mg of sea salt/liter of ultrapure water). Different concentrations of nanoparticles (5, 10, 25, 50 and 100 μg ml^{-1}) were added to the wells and incubated for 72 h at 28.5 °C. Tests were performed in duplicate and repeated thrice (60 embryos per concentration). Additional Ag$^+$ ion controls (2.5, 5, 10, 15 and 20 nM) BSA and starch controls (500 μg ml^{-1} and 1 mg ml^{-1}) were included to study the influence of Ag ions and capping agents in zebrafish embryos.

Mortality of the embryos was noted after 24, 48 and 72 h. The embryos that appeared opaque and white in color were transferred to 6 well plates along with 4 ml of the medium and incubated for 24 h. This step was essential to differentiate between malformed silver-treated embryos and dead embryos, both of which gave a white opaque appearance at 24 h post-fertilization (hpf). The dead embryos were degraded soon, whereas the structures of intact embryos were more visible by 48 hpf which allowed a clear distinction between the dead and alive. The live embryos were washed and transferred back to the test wells. The mortality rate is expressed as the total number of dead embryos after 72 hpf. Hatching rate was expressed as the number of embryos that hatched by 72 hpf, as compared to the control. Heart rate was recorded using a stopwatch at different stages (24, 48 and 72 hpf) by direct microscopic observation. The emergence of pericardial edema and phenotypic deformities were recorded. At the end of the incubation period, the embryos were anesthetized in 0.01% phenoxy ethanol and photographed using a Zeiss Axiovert 200 M equipped with an Axiocam HRc.

2.4. TEM analysis of the embryos

Embryos were incubated with 25 μg ml^{-1} of Ag-BSA nanoparticles for 48 h, decorinated, fixed in 2.5% gluteraldehyde and dehydrated. The embryos were embedded in resin (Spurr's low viscosity resin) and sectioning was done using a Reichert Jung Ultracut instrument. Ultrathin sections of tissues of interest were selected using microscopy. TEM analyses were done using a JEOL JSM 3010F and JEOL JSM 2010F and the presence of nanoparticles inside the embryo was confirmed using EDS.

2.5. Acridine orange staining

To investigate the role of apoptosis in Ag-np toxicity, acridine orange staining of nanoparticle-treated embryos was performed [16]. Acridine orange is a nucleic acid selective metachromatic dye, which emits green fluorescence upon intercalation with DNA and is widely used for detecting the sites of apoptosis in zebrafish. Acridine orange can permeate apoptotic cells and binds to DNA whereas normal cells are non-permeable to acridine orange. The embryos were transferred to Eppendorff tubes and stained with acridine orange (5 μg ml^{-1}) for 20 min at room temperature. Embryos were washed quickly in phosphate buffered saline (1 × PBS, 1st Base, Singapore) before being examining under a microscope.

2.6. 4,6-diamidino-2-phenylindole-dihydrochloride hydrate (DAPI) staining

DAPI (Roche, Basel, Switzerland) staining of the fluid inside the chorion was performed to analyze the brown color flakes found in the chorion for its identity. A working solution of (1 μg ml^{-1}) of DAPI was prepared in ethanol. Embryos at various stages were collected, the chorion was poked using a fine needle to aspirate the fluid and the embryos were transferred back to the embryo water. Slides containing the chorionic fluid were air-dried and stained with DAPI at 37 °C

for 15 min, washed twice with phosphate buffered saline (1 × PBS) and air-dried. Slides were analyzed under the DAPI filter of the microscope.

3. Results

3.1. Mortality, heart rate, edema and malformations

The nanoparticle-treated embryos showed dose-dependent toxicity under laboratory conditions. The observations were similar for both Ag-starch and Ag-BSA particles. The control groups (medium and capping agents) without the added nanoparticles appeared normal (figure 2(A)) with an overall mortality <4%. At a concentration of 5 μg ml^{-1}, the fluid inside the chorion showed slight turbidity characterized by the presence of brownish flakes (figure 2(B)). The turbidity increased with the concentration of nanoparticles and led to a white opaque appearance for the embryos (figure 2(C)). Also, the embryos had a characteristic slimy coating, which resembled mucus in texture and appearance (figure 2(D)). The DAPI staining of the chorionic fluid showed no evidence of nuclear staining in controls (figure 2(E)), whereas nanoparticle-treated embryos showed nuclear staining (figure 2(F)). The DAPI stained slimy layer showed similar patterns in both Ag-BSA and Ag-starch treatment. The LC$_{50}$ for the embryos was dependent on the growth stage (64–128 cell stage) of the embryos exposed to nanoparticle treatment, and was found to vary from 25–50 μg ml^{-1}. The later stages of the embryos were found to be more resistant to Ag-np treatment. Above 50 μg ml^{-1}, the embryos exhibited severe phenotypic changes characterized by bent and twisted notochord, accumulation of blood in the blood vessels near the tail, low heart rate, pericardial edema and degeneration of body parts. The pericardial edema was observed at 24 hpf and became more pronounced by 72 hpf.

The control embryos appeared normal throughout the test period (figure 2(G)). Occurrences of defective phenotypes were similar in both Ag-BSA (figure 2(H)) and Ag-starch (figure 2(I)). The acridine orange staining to study apoptosis showed no significant staining in control embryos (figure 2(J)), whereas the Ag-BSA (figure 2(K)) and Ag-starch (figure 2(L)) treated embryos showed green fluorescent spots on the body, which could be explained using the decomposition of body parts. The decay of the body was more obvious near the head and tail. Above a concentration of 50 μg ml^{-1}, 60–90% of the surviving embryos showed body malformations. The yolk sac of the embryos appeared distorted. The pericardial edema was prominent in most of the Ag-np treated embryos. Also, a bent notochord was common and that none of those embryos hatched out by 72 h. The heart rate of the treated embryos decreased with increase in concentration and reached an average of 39 heart beats min^{-1} above a concentration of 50 μg ml^{-1} of Ag-nps as compared to an average of 150-beats min^{-1} for the control embryos (figure 3(A)). Hatching delay was observed with increase in Ag-np concentrations. 15% of embryos were hatched with Ag-BSA (figure 3(B)) and 33% hatched with Ag-starch (figure 3(B)) nanoparticles at a concentration of 100 μg ml^{-1}. The hatching delay was
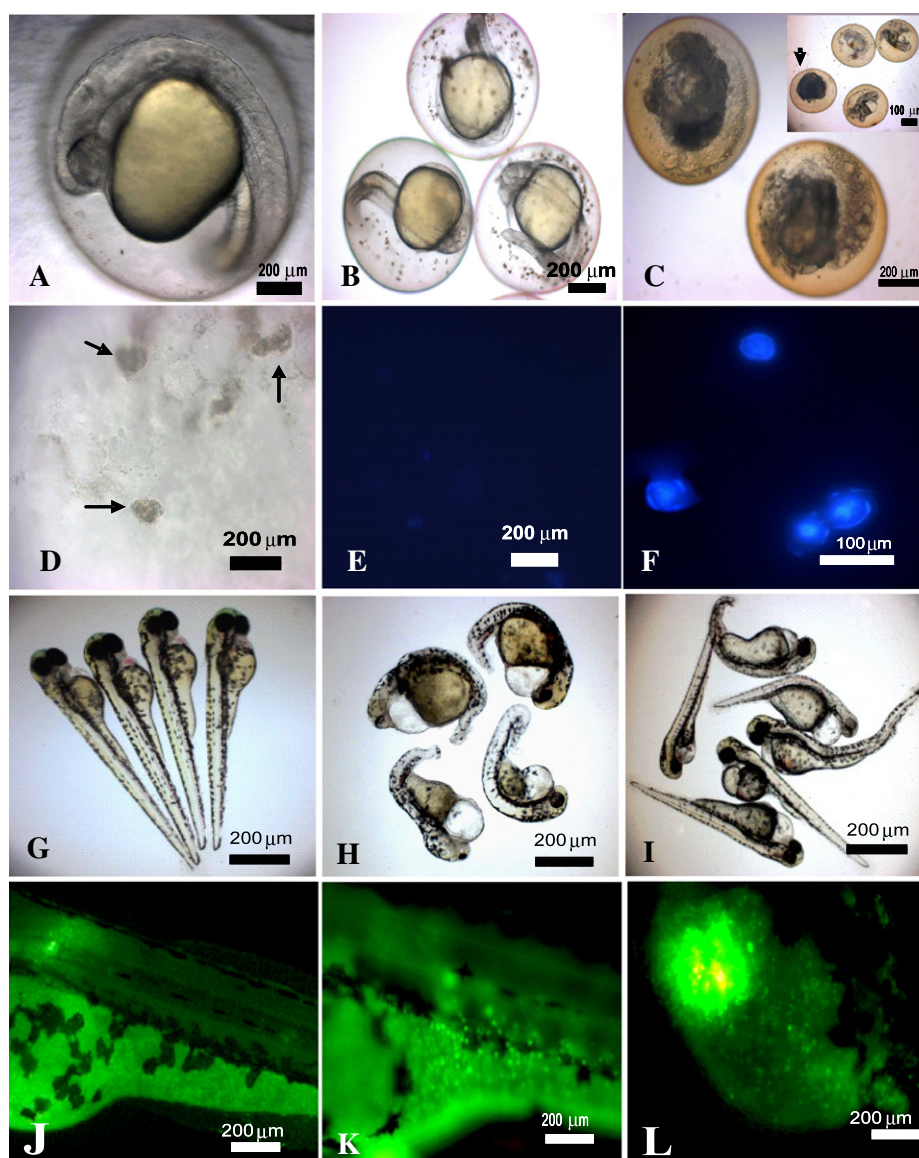
Figure 2. Microscopic images of control embryos at 24 hpf (A), which developed normally, Ag-BSA (5 μg ml^{-1}) treated embryos at 24 hpf (B) showing slimy fluid with brown flakes inside the chorion and live embryos (C) at 24 hpf showing cloudy appearance resembling dead embryos. Inset picture shows the distinct appearance of dead and malformed embryos at 48 hpf. Optical images of slimy coating with brown specks (D), isolated from the embryos (conc. of Ag-np was 10 μg ml^{-1}). DAPI-stained chorionic fluid from control embryos (E) showing no nuclear staining and slimy coating from Ag-np treated embryos (F) with clear evidence of nuclear staining. Optical micrographs of normal and healthy control larvae at 72 hpf (G), deformities in Ag-starch treated (H) and Ag-BSA treated (I) larvae (conc. 100 μg ml^{-1}). The unhatched embryos were decorinated using fine needles. Acridine orange staining (72 hpf): control embryos (J), Ag-BSA ((K) 50 μg ml^{-1}) and Ag-starch ((L) 50 μg ml^{-1}) treated embryos showing bright green spots on the skin indicating presence of apoptotic cells.

calculated from the total number of surviving embryos in each concentration with respect to the live embryos present (number of embryos hatched at 72 hpf/number of live embryos ×100; not all live embryos hatch after 72 hpf). Even though the LC$_{50}$ (concentration of Ag-np that killed 50% of the embryos) was between 25 and 50 μg ml^{-1}, a corresponding linearity in mortality was not observed at 100 μg ml^{-1}. At 100 μg ml^{-1} concentration of Ag-np, 15–30% of the embryos were still alive (figure 3(C)). No significant abnormalities were observed in embryos treated with starch and BSA alone. The heart rate and hatching were comparable with control samples, suggesting an absence of toxicity.
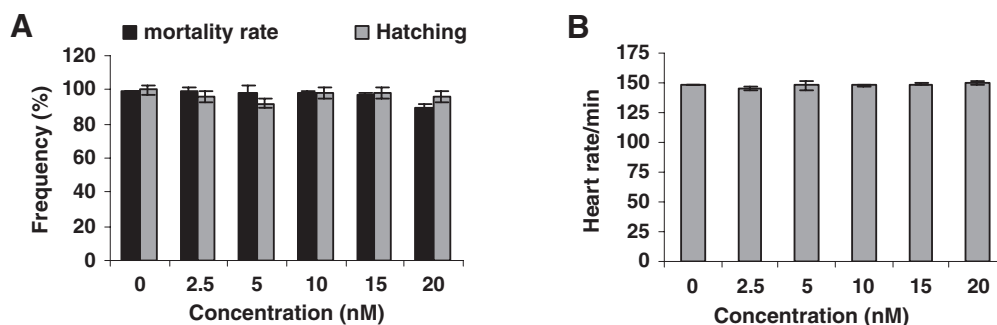
These observations were in accordance with our *in vitro* toxicity study on Ag-np, where lower concentrations had more apoptotic cells and necrotic cells than higher concentrations of Ag-np. In order to study the occurrence of apoptosis, acridine orange staining was performed for all embryos above 50 μg ml^{-1} concentrations at 72 hpf. Surprisingly, only 40–50% of the embryos exhibited bright green spots all over the body while the rest of them had a low natural fluorescence.

It can be assumed that Ag^{+} ions will get released from Ag-np under the complex physiological conditions. Hence, toxicity of Ag^{+} ions was evaluated in embryos by exposing them to silver nitrate (AgNO$_3$) solutions. Ag^{+} ions
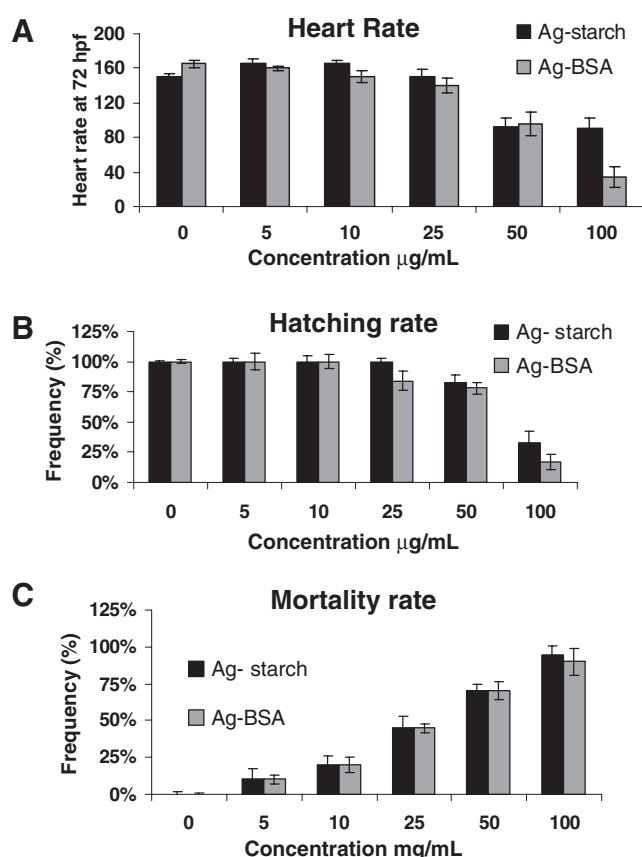
Figure 3. Graphs representing the toxicity of Ag-starch and Ag-BSA in terms of heart rate (A), hatching (B) and mortality (C). A concentration-dependent increase in mortality was observed in Ag-np treated embryos. Hatching delays and a drop in heart rate were also observed as a consequence of Ag-np treatment. The values are expressed as mean ± standard deviation of three experiments.

treated embryos showed no significant abnormalities when compared to Ag-np. The highest concentrations of Ag$^+$ ions tested (20 nM) showed 10% mortality rate whereas lower concentrations showed $\leqslant$5% mortality (figure 4(A)). Also, 4% embryos exhibited hatching delays compared to control samples. No other abnormalities were observed. Heart rates of treated embryos were comparable to controls (figure 4(B)). The overall development of the embryos was unaffected by Ag$^+$ ion treatment.
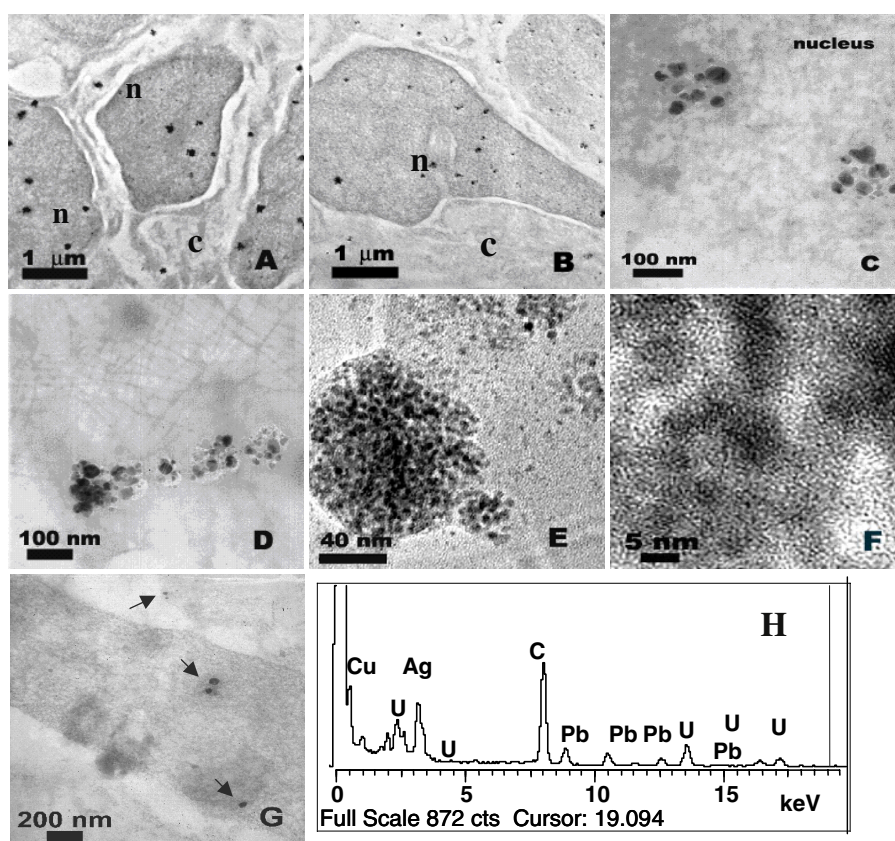
3.2. Biodistribution of Ag-BSA in zebrafish embryos

The biodistribution of nanoparticles using TEM analysis showed that the Ag-np has an affinity for the nucleus. Most of the nanoparticles were deposited inside the nucleus of the cells (figure 5(A)), whereas the cytoplasm had only a few nanoparticles (figure 5(B)). The magnified view of the nucleus showed small clumps of nanoparticles (figure 5(C)) along with depositions of nanoparticles on skin (figure 4(D)), heart (figures 5(E), (F)) and brain (figure 5(G)). However, no clumping of Ag-nps was observed inside the brain. The nanoparticles deposited inside the brain appeared to be well dispersed. Uniform distribution of nanoparticles was observed throughout the embryos. The energy-dispersive x-ray analysis (EDX) of the zebrafish tissue sections showed a significantly high concentration of silver (figure 5(H)).

4. Discussion

Silver salts are commonly used for therapeutic purposes as well as decorations in oriental pastries. Ag-np is employed in detergents and as antimicrobial agents that could end up in the environment or inside the organs of animals. Moreover, the effluents from research labs and industries carrying heavy nanoparticle content also reach environmental resources. The nanoparticles used in this study showed remarkable stability and uniform dispersion throughout the test period. No agglomeration and precipitation were observed. Nanoparticle stability is a major concern in nanotechnology and nanotoxicology. An unstable nanoparticle will precipitate to a metal clump which affects the test interpretations. In the case of water-insoluble particles the carrier solvents may exert independent toxic effects in embryos. Hence it is ideal to use water as a carrier solvent to test nanoparticle toxicity. Use of water-insoluble nanoparticles could be less effective owing to phase separation. Starch and BSA are biocompatible agents that possess the advantages of being non-toxic and good water-soluble stabilizing agents for nanoparticles.

Our results suggest the toxicity of silver nanoparticles to aquatic species depends in a concentration-dependent manner. Indicators of toxicity include drop in heart rate, high mortality rate and hatching delays observed in zebrafish embryos (figure 3). The TEM images showed that the Ag-nps have a tendency to get accumulated in the nucleus, which may lead

Figure 4. Graphs represent the effect of Ag$^+$ on embryos. (A) Mortality and hatching rate of embryos at 72 hpf. No significant hatching delay was observed in Ag$^+$ treated embryos. At 20 nM of Ag$^+$ ions, 10% mortality was observed. (B) Heart rate of embryos at 72 hpf was unaffected by Ag$^+$ ion treatment.

Figure 5. TEM images of ultrathin sections of the embryos treated with 25 μg ml^{-1} of Ag-BSA nanoparticles. Deposition of the Ag-nps in the cytoplasm (A) and nucleus (B) of the cells near the trunk and tail, respectively. Images were captured using a JEOL JSM 3010F. The nucleus is indicated by 'n' and cytoplasm by 'c'. Magnified images of the nucleus (C) showing nanoparticle deposition. Clumps of nanoparticles were seen near the epithelium (D). Low magnification images of the heart (E), showing dark spots containing nanoparticles. (F) Magnified images from heart confirming the presence of nanoparticles. The lattice plane identifies nanoparticles. (G) Sections of brain showing the presence of nanoparticles. (H) EDS of embryos showing the presence of silver.

to genomic damage and instability. It is conceivable that the nanoparticles could enter the cells through many routes, some of which include diffusion or endocytosis through the skin of embryos. This is supported by the presence of clumps of nanoparticles throughout the epidermis of the larvae. The formation of a slimy coating around the embryos may be the consequence of local injury, caused by the nanoparticles while entering the fragile skin of the embryos. An earlier report on zinc oxide nanoparticles elucidated the passage through rat and rabbit skins [17, 18]. The uniform distribution of Ag-nps could be a result of translocation of nanoparticles entering through the outer layer of the embryo. The clearance mechanisms are less effective in immature embryos, since the immune cells develop at a later stage [19]. The Ag-np was translocated to various cellular organelles from the site of entry. The nanoparticles that invade the cells during early embryonic stages, namely the four-cell stage, carry high chances of uniform distribution. It is established that these blastomeres are the precursors for various cell lineages that make up organ systems, namely the nervous system and circulatory system in mature larvae [20].

Earlier reports have shown that the nervous system could be affected by nanoparticles [21]. Nonetheless, the presence of nanoparticles in the brain of embryos does not establish

that nanoparticles are crossing the blood–brain barrier. It is possible that the nanoparticle entry during early embryonic stages resulted in a uniform distribution throughout the organ systems. However, nuclear deposition of the nanoparticles is believed to initiate a chain of toxic events. Cellular deposition of nanoparticles could have exerted stress in the form of oxidative stress [22], DNA damage [23] or proliferation delay [24]. Moreover, titanium dioxide nanoparticles were found to enhance the risk of tumor formation in rats [25].

As evident from the acridine orange staining, there was only low to moderate levels of apoptosis occurring in the embryos. Higher concentrations of Ag-nps resulted in significant growth retardation, which could be due to delay or inhibition of cell division. The Ag-np treated embryos showed a normal cardiac morphology, with atria and ventricle differentiated normally with proper orientation with time. The cardiac cycle was irregular with increase in Ag-np concentration, showing a little or no pumping of blood. Accumulation of blood in aorta near the tail and below the cardiac cavity was common, which prevented normal blood flow. Such observations suggest that the pumping of the heart was not strong enough to restore normal blood flow and Ag-nps were interfering with the normal activity of cardiac muscles either directly or by blocking the energy sources that influence

the smooth functioning of the system. Blood flow cutoff must have forced the cells to be starved out of essential nutrients and gases, which ultimately leads to decomposition of the body. A proper blood flow to the brain and spinal chord is a critical event in the survival of the larvae. Nanoparticles are known to interact with the vascular endothelium or have direct effects on atherosclerotic plaque [26] or act as a site for thrombus formation [27, 28] and myocardial infarctions [29]. The observed insensitivity of the larvae to touch leads to a suspicion of a neurological disorder amplified by the absence of blood flow. The fluid imbalance is believed to be a contributing factor in bent body axis; so is the deposition of nanoparticles in the brain. The nanoparticle deposition in the brain could interfere with functioning of the nervous system and signal transduction processes. The nanoparticle could act as a foreign body, restricting the normal activity of the cell or organ where it is deposited. It is conceivable that, under such circumstances, the larvae are not expected to survive. The observed hatching delays and abnormal body axis restricts the chances of survival. The non-toxicity of BSA and starch controls showed that the observed effects are specifically mediated by Ag-np. Ag^+ ions have been reported to have toxicity in aquatic species. Ag ions treatment induced ion regulatory impairment and increased mortality in rainbow trout eggs [30]. The Ag-nps used for this study were washed many times in ultrapure water to ensure complete removal of residual capping agents and Ag ions. It is believed that Ag^+ ions get released by the surface oxidation of Ag-np under the complex physiological conditions *in vivo* that can influence the properties of silver nanoparticles such as antimicrobial activity [31]. We used Ag^+ ions and Ag nanoparticles to compare the occurrence of phenotypic defects. None of the phenotypic defects observed in Ag-np treatment were observed in the case of Ag^+ ions treated embryos. This suggests that Ag-np mediated toxicity is not due to the presence of Ag^+ ions in the medium.

Throughout the experiments, the dependence of the growth stage to the toxic parameters was observed. The mortality rate was high in embryos treated with Ag-np at 2–8 cell stages, whereas, embryos entering epiboly (4–6 hpf) were more resistant. There have been reports on the toxicity of fullerenes (C60) and its variants in aquatic species, which resulted in oxidative stress and lipid peroxidation [32]. Similar mechanisms are possible with Ag-np and thus will be the focus for future studies.

5. Conclusion

We conclude that the Ag-nps have the potential to cause health and ecotoxicity in a concentration-dependent manner. The Ag-np treated embryos exhibited phenotypic defects, altered physiological functions, namely bradycardia, axial curvatures and degeneration of body parts. Clumps of nanoparticles were seen throughout the epidermis of the larvae confirming the aberrations of skin caused by the Ag-np. The presence of a slimy coating is believed to be a result of nanoparticle entry through the abraded skin of the embryos. The TEM images showed the presence of nanoparticles in the brain of the embryos. Nanoparticle deposition in the

central nervous system could have deleterious effects, by negatively controlling the cardiac rhythm, respiration and body movements. The pathological events following long-term deposition of nanoparticles in the nervous system and other organs remain unclear. It is expected that the deposition of nanoparticles inside the nucleus of the cells led to the observed toxicity through various mechanisms such as DNA damage and chromosomal aberrations. Furthermore, the exposure of Ag-np resulted in accumulation of blood in different parts of the body, thereby causing edema and necrosis. Further studies will be directed towards the genotoxicity and the gene expression profile of Ag-np treated embryos. This study pointed out the adverse effects of Ag-np in aquatic species and all applications involving silver nanoparticles should be given special attention and promoted only after detailed studies. The release of untreated nanoparticle waste to the environment should be restricted for the well being of human and aquatic species.

Acknowledgments

References

[1] Perugini P, Simeoni S, Scalia S, Genta I, Modena T, Conti B and Pavanetto F 2002 Effect of nanoparticle encapsulation on the photostability of the sunscreen agent, 2-ethylhexyl-p-methoxycinnamate *Int. J. Pharm.* **246** 37–45

[2] Jin S and Ye K 2007 Nanoparticle-mediated drug delivery and gene therapy *Biotechnol. Prog.* **23** 32–41

[3] Czupryna J and Tsourkas A 2006 Suicide gene delivery by calcium phosphate nanoparticles: a novel method of targeted therapy for gastric cancer *Cancer Biol. Ther.* **5** 1691–2

[4] Prow T, Grebe R, Merges C, Smith J, McLeod S, Leary J and Lutty G 2006 Nanoparticle tethered biosensors for autoregulated gene therapy in hyperoxic endothelium *Nanomedicine* **2** 276

[5] Yoon K Y, Hoon-Byeon J, Park J H and Hwang J 2007 Susceptibility constants of *Escherichia coli* and *Bacillus subtilis* to silver and copper nanoparticles *J. Sci. Total Environ.* **373** 572–5

[6] Tian J, Wong K K, Ho C M, Lok C N, Yu W Y, Che C M, Chiu J F and Tam P K 2007 Topical delivery of silver nanoparticles promotes wound healing *Chem. Med. Chem.* **2** 129–36

[7] Asz J, Asz D, Moushey R, Seigel J, Mallory S B and Foglia R P 2006 Treatment of toxic epidermal necrolysis in a pediatric patient with a nanocrystalline silver dressing *J. Pediatr. Surg.* **41** 9–12

[8] Zhang Q, Kusaka Y, Zhu X, Sato K, Mo Y, Kluz T and Donaldson K 2003 Comparative toxicity of standard nickel and ultrafine nickel in lung after intratracheal instillation *J. Occup. Health* **45** 23–30

[9] Obserdorster E 2004 Manufactured nanomaterials (fullerenes, C60) induce oxidative stress in the brain of juvenile largemouth bass *Environ. Health Perspect.* **112** 1058–62

[10] Kashiwada S 2006 Distribution of nanoparticles in the see-through medaka (*Oryzias latipes*) *Environ. Health Perspect.* **114** 1697–702

[11] Braydich-Stolle L, Saber H, Schlager J J and Hofmann M-C 2005 *In vitro* cytotoxicity of nanoparticles in mammalian germline stem cells *Toxicol. Sci.* **88** 412–9

[12] Hussain S M, Hess K L, Gearhart J M, Geiss K T and Schlager J J 2005 *In vitro* toxicity of nanoparticles in BRL 3A rat liver cells *Toxicol. In Vitro* **19** 975–83

[13] Skebo J E, Grabinski C M, Schrand A M, Schlager J J and Hussain S M 2007 Assessment of metal nanoparticle agglomeration, uptake, and interaction using high-illuminating system *Int. J. Toxicol.* **26** 135–41

[14] Thomas S, Nair S K, Jamal E M A, Al-Harthi H S, Varma M R and Anantharaman M R 2008 Size dependant surface plasmon resonance in silica silver nanocomposites *Nanotechnology* **19** 075710

[15] Westerfield M 2000 *The Zebrafish Book. A Guide for the Laboratory use of Zebrafish (Danio rerio)* vol 4 (Eugene: Univ. of Oregon Press)

[16] Detrich H W, Westerfield M and Zon L I 2004 Methods in cell biology *The Zebrafish Cellular and Developmental Biology* vol 76 (California: Elsevier)

[17] Hallmans G and Liden S 1979 Penetration of 65Zn through the skin of rats *Acta Dermatol. Venereol.* **59** 105–12

[18] Kapur S P, Bhussry B R, Rao S and Hormouth-Hoene E 1974 Percutaneous uptake of zinc in rabbit skin *Proc. Soc. Exp. Biol. Med.* **145** 932–7

[19] Trede N S, Langenau D M, Traver D, Look A T and Zon L I 2004 The use of zebrafish to understand immunity *Immunity* **20** 367–79

[20] Solnica-Krezel L 2002 *Pattern Formation in Zebrafish* (Heidelberg: Springer)

[21] Oberdorster G, Sharp Z, Atudorei V, Elder A, Gelein R, Kreyling W and Cox C 2004 Translocation of inhaled ultrafine particles to the brain *Inhal. Toxicol.* **16** 437–45

[22] Xia T, Kovochich M, Brant J, Hotze M, Sempf J, Oberley T, Sioutas C, Yeh J I, Wiesner M R and Nel A E 2006 Comparison of the abilities of ambient and manufactured nanoparticles to induce cellular toxicity according to an oxidative stress paradigm *Nano Lett.* **6** 1794–807

[23] Wang J J, Sanderson B J S and Wang H 2007 Cyto- and genotoxicity of ultrafine TiO_2 particles in cultured human lymphoblastoid cells *Mutat. Res.* **628** 99–106

[24] Pernodet N, Fang X, Sun Y, Bakhtina A, Ramakrishnan A, Sokolov J, Ulman A and Rafailovich M 2006 Adverse effects of citrate/gold nanoparticles on human dermal fibroblasts *Small* **2** 766–73

[25] Lee K P, Henry N W 3rd, Trochimowicz H J and Reinhardt C F 1986 Pulmonary response to impaired lung clearance in rats following excessive TiO_2 dust deposition *Environ. Res.* **41** 114–67

[26] Kumar C 2006 *Nanomaterials—Toxicity, Health and Environmental Issues* vol 5 (Weinheim: Wiley–VCH)

[27] Khandoga A, Stampefl A, Takenaka S, Schulz H, Radykewicz R, Kreyling W and Krombach F 2004 Ultrafine particles exert prothrombotic but not inflammatory effects on the hepatic microcirculation in healthy mice *in vivo Circulation* **109** 1320–5

[28] Gatti A M, Montanari S, Monari E, Gambarelli A, Capitani F and Parisini B 2004 *J. Mater. Sci. Mater. Med.* **15** 469–72

[29] Peters A, Dockery D W, Muller J E and Mittleman M A 2001 Increased particulate air pollution and the triggering of myocardial infarction *Circulation* **103** 2810–5

[30] Guadagnolo C M, Brauner C J and Wood C M 2000 Effects of an acute silver challenge on survival, silver distribution and ionoregulation within developing rainbow trout eggs (*Oncorhynchus mykiss*) *Aquat. Toxicol.* **51** 195–211

[31] Lok C N, Ho C M, Chen R, He Q Y, Yu W Y, Sun H, Tam P K, Chiu J F and Che C M 2007 Silver nanoparticles: partial oxidation and antibacterial activities *J. Biol. Inorg. Chem.* **12** 527–34

[32] Zhu S, Oberdorster E and Haasch M L 2006 Toxicity of an engineered nanoparticle (fullerene, C60) in two aquatic species, Daphnia and fathead minnow *Mar. Environ. Res.* **62** S5–9